Linking shifts in bacterial community with changes in dissolved organic matter pool in a tropical lake

Avila, Marcelo P.

2019-07-01

Avila , M P , Brandao , L P M , Brighenti , L S , Tonetta , D , Reis , M P , Staehr , P A , Asmala , E , Amado , A M , Barbosa , F A R , Bezerra-Neto , J F & Nascimento , A M A 2019 , ' Linking shifts in bacterial community with changes in dissolved organic matter pool in a tropical lake ' , The Science of the Total Environment , vol. 672 , pp. 990-1003 . https://doi.org/10.1016/j.scitotenv.20

http://hdl.handle.net/10138/328897
https://doi.org/10.1016/j.scitotenv.2019.04.033

Linking shifts in bacterial community with changes in dissolved organic matter pool in a tropical lake

Marcelo P. Ávila[1], Luciana P. M. Brandão[1], Ludmila S. Brighenti[1], Denise Tonetta[1], Mariana P. Reis[1], Peter A. Staehr[2], Eero Asmala[2, 3], André M. Amado[4], Francisco A. R. Barbosa[1], José F. Bezerra-Neto[1], Andréa M. A. Nascimento[1]*

[1]Departamento de Biologia Geral, Instituto de Ciências Biológicas, Universidade Federal de Minas Gerais, Belo Horizonte, MG 31270-901, Brazil

[2]Department of Bioscience, Aarhus University, Frederiksborgvej 399, Box 358, 4000 Roskilde, Denmark

[3]Tvärminne Zoological Station, University of Helsinki, J.A. Palménin tie 260, 10900 Hanko, Finland

[4] Limnology Laboratory, Department of Oceanography and Limnology, Universidade Federal do Rio Grande do Norte, Rio Grande do Norte, Brazil,

*Corresponding author: Andréa M. A. Nascimento. Institutional address: Avenida Antônio Carlos 6627, 31270-901, Belo Horizonte, MG, Brazil. Phone: +55 31 3409 2588; fax: +55 31 3409 2567; e-mail: amaral@ufmg.br

Abstract

Bacterioplankton communities have a pivotal role in the global carbon cycle. Still the interaction between microbial community and dissolved organic matter (DOM) in freshwater ecosystems remains poorly understood. Here, we report results from a 12-day mesocosm study performed in the epilimnion of a tropical lake, in which inorganic nutrients and allochthonous DOM were supplemented under full light and shading. Although the production of autochthonous DOM triggered by nutrient addition was the dominant driver of changes in bacterial community structure, temporal covariations between DOM optical proxies and bacterial community structure revealed a strong influence of community shifts on DOM fate. Community shifts were coupled to a successional stepwise alteration of the DOM pool, with different fractions being selectively consumed by specific taxa. Typical freshwater clades as *Limnohabitans* and *Sporichthyaceae* were associated with consumption of low molecular weight carbon, whereas Gammaproteobacteria and Flavobacteria utilized higher molecular weight carbon, indicating differences in DOM preference among clades. Importantly, *Verrucomicrobiaceae* were important in the turnover of freshly produced autochthonous DOM, ultimately affecting light availability and dissolved organic carbon concentrations. Our findings suggest that taxonomically defined bacterial assemblages play definite roles when influencing DOM fate, either by changing specific fractions of the DOM pool or by regulating light availability and DOC levels.

Keywords:

Community structure, bacterioplankton, CDOM, mesocosm, Verrucomicrobiaceae

Introduction

Bacteria are key components of aquatic ecosystems playing crucial roles in biogeochemical cycles and ecosystem functioning (Lindeman, 1942; Pernthaler, 2005). Due to their metabolic diversity, morphology, large biomass, and high turnover rates, bacteria respond quickly to changes in catchments and associated water, affecting carbon cycling and energy transfer to higher levels in aquatic food webs (Cotner and Biddanda, 2002; Sanders et al., 2015). Freshwater ecosystems are exposed to a variety of stressors related to anthropogenic activities like elevated nutrient inputs and increases in organic matter runoff (Carpenter et al., 2011). Associated with such impacts are changes in rates of aquatic primary production and respiration, and alterations in the overall flux of carbon and composition of dissolved organic matter (DOM) (Bocaniov et al., 2013; Brandão et al., 2018). Despite differences in molecular size and degradability (Hansen et al., 2016), both autochthonous and allochthonous DOM fuel bacterial metabolism, affecting the availability of inorganic nutrients and organic carbon ultimately determining if autotrophic or heterotrophic energy mobilization will prevail (Jansson et al., 2007; Berglund et al., 2007).

The autochthonous DOM mainly consists of simple molecules (carbohydrates, proteins and amino acids) of low molecular weight (LMW) and is typically more labile for microbial community (Farjalla et al., 2009; Fonte et al., 2013). On the other hand, the allochthonous DOM is more susceptible to photodegradation because it contains relatively large molecules with high numbers of aromatic compounds, which strongly absorb UV light (Amon and Benner, 1994; McKnight et al., 1994; Benner, 2002; Helms et al., 2008). In this context, the chromophoric fraction of DOM (CDOM) constitutes an important and very variable pool of carbon, consisting of a continuum from labile to recalcitrant constituents (Rochelle-Newall et al., 2004, Benner and Amon, 2015). Bacterioplankton can increase the

amount of CDOM by transforming non-colored autochthonous DOM (Nelson et al., 2004; Asmala et al., 2018). Previous studies show that BCS varies with DOM composition and suggest ecological coherence between BCS and DOM composition (Judd et al., 2006; Amaral et al., 2016; Sarmento et al., 2016). While community adaption (*i.e.* composition shifts) has been found to precede bacterial degradation of specific carbon substrates (Cory and Kling, 2018), the contribution of BCS shifts and key bacterial players in the production and degradation of CDOM is unclear (Zhang et al., 2018).

Spectrophotometric analysis of CDOM is an important tool in studies of composition and origin of organic matter (Helms et al., 2008; Massicotte et al., 2017). Metrics extracted from the CDOM absorbance spectrum provide information on aromaticity ($SUVA_{254}$; Weishaar et al., 2003), changes in relation to photo- ($S_{275-295}$) and biodegradation ($S_{350-400}$) (Helms et al., 2008), and changes in the relative size of DOM molecules (a_{250}: a_{365}; De Haan and De Boer, 1987). Brandão et al. (2018) similarly used DOM optical proxies to infer a range of quantitative and qualitative changes observed during a factorial mesocosm experiment employing additions of allochthonous DOM and inorganic nutrients. Their results indicated that additions of allochthonous DOM affected CDOM absorption in the PAR range, with high influence of photodegradation. In contrast, more labile autochthonous DOM was degraded by bacteria, as suggested by Berggren et al. (2009).

Here, we applied a high-resolution taxonomic community analysis to characterize changes in the bacterioplankton and link this to the dynamics of the DOM pool documented by Brandão et al. (2018). By relating our findings to the DOM optical proxies described above, and results from the same mesocosm experiment (Tonetta et al., 2018; Brighenti et al., 2018), we aimed to provide insights on the interaction between DOM and BCS. By tracking down taxonomic signatures associated with specific changes in DOM, we expect a high degree of resource partitioning among bacterioplankton, as previously suggested for marine

99 waters (McCarren et al., 2010; Sarmento et al., 2016). This presumption is endorsed by the
100 great bacterioplankton diversity previously observed in the studied lake (Ávila et al., 2017).
101 Additionally, the effect of direct and reduced sunlight was considered to investigate how
102 photodegradation affects the association between BCS and DOM properties.
103
104 **Methods**
105 **Study area**
106 The data from this study originates from the mesocosm experiment described in detail
107 by Brandão et al. (2018). In summary, the experiment was carried out in Lake Carioca
108 (19°45'26.0''S; 42°37'06.2''W) located in the Rio Doce State Park, a remnant protected area
109 of the Atlantic Forest (Minas Gerais, Brazil). This conservation unity is of great importance
110 for global maintenance of biological diversity (http://www.ramsar.org). Lake Carioca is a
111 small (perimeter: 1,718 m, area: 0.14 km^2, volume: 671 x 10^3 m^3, maximum depth: 11.8 m,
112 mean depth: 4.8 m; Bezerra-Neto et al., 2010), turbid, mesotrophic and monomictic lake. The
113 experiment was carried out in January, when Lake Carioca waters are found to be stratified
114 (from September to April), increasing the lake euphotic zone depth and water transparency
115 (Barbosa et al., 2012). Further characteristics of Lake Carioca can be found elsewhere
116 (Brighenti et al., 2015; Reis et al., 2016).
117
118 **Mesocosm setup and water physico-chemical characterization**
119 The experiment was planned to mimic seasonal changes in inputs of allochthonous
120 DOM and nutrients associated with variability in rain, water level and litter fall. It was
121 carried out during summer 2015 (20th January to 1th February). Mesocosms (1.5 m height, 1.3
122 m diameter and volume 2 m^3) were installed in the upper mixed zone of the lake. The
123 experiment applied a 2^3 factorial design with different combinations of inorganic nutrients

and allochthonous DOM additions and shading in two replicates each, totalizing 16 mesocosms (Fig. S2). Each mesocosm was named according to the allochthonous DOM (C), inorganic nutrient (N), and light (L) in that particular order (*e.g.*, additions of allochthonous DOM and nutrient under shading: $C^{+}N^{+}L^{-}$). Inorganic nutrient additions consisted of initial inoculation with nitrate (6.1 g of $NaNO_3$), ammonium (0.42 g of NH_4Cl) and phosphate (1.15 g of K_2HPO_4) diluted in 40 ml of distilled water, resulting in initial concentrations of 2,575 µg NO_3^{-} L^{-1}, 71 µg NH_4^{+} L^{-1} and 160 µg PO_4^{-3} L^{-1} at the amended bags. The allochthonous DOM consisted of fallen leaves, plant detritus and soil particles collected from forest floor bordering Lake Carioca. The litter material was dark-incubated for seven days at room temperature (32°C) in buckets filled with 60 L of distilled water without nutrient supplementation. Following, the admixture was filtered on a 62 µm mesh and 7.5 L of the filtrate were added in C^{+} treatments, resulting in an initial concentration of 8.6 mg DOC L^{-1}. To study the influence of the light availability in the mesocosms a shade net was placed reducing 50% of light irradiance. The efficacy of light attenuation was confirmed using a radiometer BIC (Biospherical Instruments, United States of America). The DOM proxies assessed were absorbance at 350 nm (a_{350}), spectral slopes between 275-295 nm ($S_{275-295}$) and 350-400 nm ($S_{350-400}$), DOC and its normalized absorbance at 254 nm (SUVA) and diffuse PAR attenuation coefficient (K_{dPAR}). a_{350} is a quantitative proxy of photo-absorbing DOM (De Haan and De Boer, 1987), $S_{275-295}$ and $S_{350-400}$ are qualitative indicators of photo- and biodegradable CDOM, respectively, and values are inversely proportional to CDOM molecular weight (Helms et al., 2008). SUVA indicates DOM aromaticity (Weishaar et al., 2003) and K_{dPAR} is inversely proportional to the availability of light in the PAR range (Kirk 1994), being both quantitative and qualitative proxies. All measurements and calculations were made as described by Brandão et al. (2018), except for K_{dPAR} (Brandão et al., 2016).

Detailed information on the experimental design and measurements are described by Brighenti et al. (2018) and Tonetta et al. (2018).

Sample collection

Water samples (250 ml) from all 16 mesocosms were taken on days 1, 2, 3, 6, 9 and 12, whereas on day 0 only the control (C^-) and allochthonous DOM added (C^+) mesocosms were sampled, as nutrient was added aseptically. Thus, we considered that initial differences in microbial communities were limited to microbes inoculated via allochthonous DOM addition. Samples were immediately transported to the laboratory, filtered (0.22 μm, Millipore, Billerica, MA, USA) and stored at -20ºC until DNA extraction.

DNA extraction, library construction, sequencing and qPCR

Total DNA was extracted using the E.Z.N.A. ® Soil DNA Kit (OmegaBio-Tek) as recommended by the manufacturer and quantified with the Qubit fluorometer (Invitrogen-Life Technologies, USA). Following DNA isolation, paired-end libraries were constructed to assess the bacterial community composition using the primers S-D-Bact-0341-b-S-17/S-D-Bact-0785-a-A-21 (Klindworth et al., 2013), with Illumina adapters added, which target the V3-V4 regions of the 16S rRNA gene. The paired-end sequencing of the libraries was performed in an Illumina MiSeq platform (San Diego, CA, USA).

In order to assess the bacterial abundance, the 16S rRNA gene was estimated using the primer set 338F (5'TACGGGAGGCAGCAG3') (Lane et al., 1991) and 518R (5'ATTACCGCGGCTGCTGG3') (Muyzer et al., 1993), and the ABI 7900HT Fast Real-Time PCR System. (Applied Biosystems, Foster City, CA). Reaction conditions were as described by Reis et al. (2013).

Bioinformatics

After sequencing, raw reads were merged and processed using MOTHUR v.1.34.4 (Schloss et al., 2009), including quality filtering (length < 400 and >430, without ambiguities and homopolymers > 8), chimera check and singleton exclusion using UCHIME (Edgar et al., 2011). The remaining reads were aligned and classified against the SILVA v.123 database (Quast et al., 2013) and clustered into operational taxonomic units (OTUs) using 3% as dissimilarity cutoff. Reads not classified into the Bacteria domain were removed (3 reads, representing $<10^5$% of total).

Data analysis

All statistical analyses were performed in R (https://www.r-project.org - R Core Team 2018) and the main steps performed are summarized in Figure S3. For alpha and beta diversity (PCoA) analyses reads assigned as Cyanobacteria and chloroplasts were removed from the dataset. Alpha diversity metrics (OTU richness and Simpson Evenness index) were determined after random normalization of reads counts at 1,629 reads depth. Changes in 16S abundance measures, alpha and beta diversity (described below), and DOM proxies were assessed using multiple linear regression analysis considering time, allochthonous DOM and nutrient additions and shade as explanatory variables, contemplating also first-order interactions. In order to evaluate regular time intervals and adjust community data to the same sampling frequency of DOM-related data, only samples from days 0, 3, 6, 9 and 12 were considered. The percentages of Cyanobacteria and chloroplasts, which are derived from eukaryotic phototrophs, were calculated using the sum of the relative frequency of all reads classified as members of these groups, the remaining reads were assumed to represent bacterioplankton.

For Principal Coordinate Analysis (PCoA), beta diversity was calculated using all samples with more than 2,000 reads (3 out of 99 samples were removed: $C^{-}N^{+}L^{+}$ day 12, $C^{+}N^{-}L^{+}$ day 3 and $C^{+}N^{+}L^{-}$ day 9). After pruning these samples, a mean sample size of 57,562 reads was observed. The normalization of reads per sample was based on cumulative sum scaling, as implemented by metagenomeSeq (Paulson et al., 2013), which conserves the relative proportion of species. Normalized OTU counts were further squared-root transformed and dissimilarity was calculated using weighted UniFrac distances (Lozupone et al., 2005) using the R-package phyloseq (McMurdie and Holmes, 2013). The input tree used for UniFrac distance calculation was generated in MOTHUR with the clearcut program (Evans et al., 2006), using the most abundant representative sequence of each OTU. The sample and OTU scores of the first three principal coordinates were subsequently extracted. The same procedure used to model the environmental variables was used to evaluate the relationship between the sample scores (response variable) and time, allochthonous DOM and nutrient additions and shade (explanatory variables).

To evaluate the synchronism in changes of DOM and BCS, a causality diagram was created to compare the outcomes from switching DOM proxies and principal coordinates extracted from the PCoA as factor and determinant on each other. Hence, it was tested whether temporal shifts in one type of variable (ΔPCoA or ΔDOM) were correlated with preceding ($PCoA^{initital}$ or $DOM^{initial}$) or subsequent ($PCoA^{final}$ or DOM^{final}) levels of the other type of variable. Correlations likely indicate synchrony and were used to reveal positive and negative stimuli between community gradients (PCoA axis) and DOM proxies. This was done by comparing all possible combinations of linear regressions tested between DOM proxies and scores of the three main PCoA's axes: changes within a three-day interval in one hand ($\Delta PCoA^{0-3}$ and ΔDOM^{0-3} - response variable) versus either levels of the explanatory variable immediately before ($PCoA^{0}$ and DOM^{0}), or after ($PCoA^{3}$ and DOM^{3}) the three-day

shift. Resultant significant linear regressions (p-value < 0.05) exhibiting a coefficient of determination (R^2) > 0.2 were further considered and summarized in the causality diagram. The time interval of three days was chosen based on results from an experiment performed during field campaign in which carbon lability was inferred from daily changes of pCO_2 levels in dark incubations at 30ºC, similar to lake conditions. Within three days, all treatments except one ($C^+N^+L^+$) had achieved maximum carbon remineralization, as pCO_2 reached the highest values, decreasing afterwards (Fig. S4).

To identify the taxonomic groups associated with each PCoA axis, the dispersion of OTU scores was inspected at different taxonomic levels. Plots were made to show the most abundant taxa considering pre-determined cut-offs of OTU richness per hierarchy, as follow 30, 25, 15 and 10 for phylum, class, family and genus, respectively. An additional selection for a class final plot considered the five highest and lowest mean scores presented by taxon for all PCoA axes, whereas for family and genus, the eight highest and lowest mean scores were selected for each axis. Plots were drawn using the geom_violin function in the ggplot2 package (Wickham et al., 2016), a feasible way to incorporate the density (i.e., indicating number of OTUs) along axis scores, thus illustrating the PCoA axis scores interval which a given taxon displays increased OTU richness. Finally, in order to reduce the number of taxa displayed and depict the distribution of OTUs over the three PCoA axis in an easily comparable fashion, trilinear plots were built using the function ggtern (Hamilton and Ferry, 2018). The taxa chosen for the plots represented the 12 (phylum and class) and 16 (family and genus) bacterial groups, which better illustrated the different occurrence patterns observed for each hierarchic level. Each plot shows all OTUs of a given taxonomy in relation to their normalized PCoA species scores: PCoA1 + PCoA2 + PCoA3 = 1 (100%). Colored areas represent the OTUs distribution density according to a Gaussian kernel estimator implemented in the stat_density_tern function in ggtern.

All sequences were submitted to the Sequence Read Archive (http://www.ncbi.nlm.nih.gov/sra/) under the BioProject ID PRJNA515842.

Results

Changes in microbial characteristics and DOM-related proxies

The effect of shading and additions of nutrient and allochthonous DOM on microbial aspects (*i.e.* 16S abundance, richness, evenness and relative abundance of heterotrophs and phototrophs) of the mesocosms are shown in Figure 1 and Table 1. We did not observe influence of light in microbial measurements ($p>0.05$). C^+ and N^+ mesocosms presented similar increases in 16S mean abundance (331.0 and 291.1%, respectively). Community richness was higher in C^+ mesocosms (25.5%), particularly at the beginning of the experiment due to the inoculation of allochthonous DOM-associated microbes. However, a reduction over time (-1.9% per day) was observed, thereby neutralizing the initial enrichment. Bacterioplankton relative abundance and community evenness diminished in N^+ treatments over time (-2.9% and -3.1% per day, respectively), with strongest effects on bacterioplankton relative abundance. The relative abundance of Cyanobacteria was reduced by allochthonous DOM addition (-5.8% per day) and increased by nutrient addition (5.3% per day). The relative abundance of chloroplasts was also reduced in treatment C^+ (-86.0%) and increased in N^+ (65.3%) considering total changes, however both additions caused daily increases of 18.0 and 8.4%, respectively.

Differently from microbial parameters, changes in DOM optical properties to manipulations were overall stronger and significant for all treatments, including shading (Fig. 2 and Table 2). Allochthonous DOM addition strongly decreased the $S_{275\text{-}295}$ (-13.3%) and $S_{350\text{-}400}$ (-6.5%) proxies and increased the DOC levels (8.7%), SUVA (17.2%) and a_{350}

271 (56.5%) proxies. Nutrient addition increased a_{350} (9.1%) and decreased $S_{275-295}$ (-2.2%),
272 meanwhile shading contributed for a reduction of $S_{275-295}$ (-0.3% per day), $S_{350-400}$ (-1.1%)
273 and increase in a_{350} (9.1% in N^- treatments, only).
274
275 **Bacterioplankton community structure**
276 Changes in BCS, assessed through a PCoA, showed that nutrient and allochthonous
277 DOM additions affected community structure differently, while the effect of shading was
278 inconclusive (Fig. 3). Allochthonous DOM addition promoted changes in BCS on day zero.
279 This effect seems to have persisted in absence of nutrient supplementation, as the
280 dissimilarity between N^-C^+ and N^-C^- treatments was observed throughout the experiment. In
281 contrast, pronounced changes observed in N^+ treatments over time resulted in more similar
282 communities, despite the allochthonous DOM addition. Between days 6 and 12, the N^+
283 communities experienced notable changes, segregating from N^- communities towards high
284 PCoA1 and 2 scores.
285 The three main principal coordinates accounted for 57.5% of community variation
286 (Fig. S5 and Table 3). PCoA1 was mainly influenced by the interaction between time and
287 nutrient addition, increasing with a daily rate of 42.4%. A minor gain over time was also
288 caused by allochthonous DOM addition (11.7% per day), as well as by time alone (10.5% per
289 day). PCoA2 had a complex pattern of variance, mainly influenced by allochthonous DOM
290 and nutrient additions. Initially, axis 2 was augmented in C^+ treatments, however, as the
291 scores suddenly decreased until day three, the overall effect of allochthonous DOM addition
292 was weak and non-significant. Moreover, scores tended to diminish over time (-7.3% per
293 day), except for N^+ treatments, which increased at a daily rate of 9.2%. Differently from the
294 other axes, in which a large score variation occurred during initial (PCoA2) or late (PCoA1
295 and 2) periods, PCoA3 exhibited a pattern of variance defined by a scores' peak occurring on

296 day 3 and a second peak close to day 12. Although the effect of allochthonous DOM addition
297 was not significant, the highest peak of PCoA3 scores was achieved in treatment C^+N^+,
298 reflecting a further stimulation by allochthonous DOM addition.
299
300 **Linking DOM proxies and changes in BCS**
301 The assessment of synchrony in changes of the carbon pool and BCS suggested that
302 the influence of BCS on DOM fate (Table 4, $\Delta PCoA^{0\text{-}3} \sim DOM^3$ and $\Delta DOM^{0\text{-}3} \sim PCoA^0$) was
303 stronger than microbial adaptation in response to DOM (Table 5, $\Delta PCoA^{0\text{-}3} \sim DOM^0$ and
304 $\Delta DOM^{0\text{-}3} \sim PCoA^3$). Whereas quantitative DOM proxies as DOC and K_{dPAR} were both
305 associated with PCoA1 and 3, qualitative proxies such as $S_{350\text{-}400}$ were linked to PCoA2 and
306 3, suggesting a disjuncture in the relationship between DOM and BCS (Tables 4 and 5). The
307 optical proxies a_{350}, SUVA (both associated with PCoA3) and $S_{275\text{-}295}$ (PCoA2) correlated to
308 one principal coordinate each, indicating constricted associations with the bacterioplankton
309 community. Therefore, PCoA1 was related to quantitative and PCoA2 was related to
310 qualitative measures of DOM, while PCoA3 was related to both qualitative and quantitative
311 proxies. Moreover, PCoA3 yielded stronger correlations with a larger number of proxies than
312 the two other axes, likely representing a community fraction highly committed with DOM
313 variation.
314 Figure 4 illustrates positive and negative associations between BCS and DOM-related
315 proxies, as well as the effect of shading on these interactions. The spectral slopes were
316 positively influenced by prior shifts in PCoA2. Decreases in $S_{350\text{-}400}$, which is a proxy related
317 to biodegradable DOM, and increases in CDOM (a_{350}) anticipated high PCoA3 scores. The
318 influences of PCoA2 on $S_{350\text{-}400}$ (R^2=0.46 and p=0.003) and of $S_{350\text{-}400}$ (R^2=0.37 and p=0.002)
319 and a_{350} (R^2=0.27 and p=0.01) on PCoA3 were more predictable under shading (Figs. S6 and
320 S7). PCoA3 was the major regulator of DOM-associated properties, affecting also DOM

aromaticity (SUVA) and quantity (DOC). The reason why the relationship between DOC levels and PCoA3 seemed dubious (Fig. 4), may be the pulse-like variation of PCoA3 scores over time (Fig. S5). Across the time series, PCoA3 peaks coincided with minimum DOC levels in most treatments (Fig. 2). Likewise, while high DOC levels anticipated gain of PCoA3 scores, increasing PCoA3 resulted in subsequent low DOC levels. Thus, the DOC increase observed after high PCoA3 scores was a consequence of the recovery of DOC levels posterior to high abundances of high-PCoA3 bacteria. Therefore, our results indicate that PCoA3 pulses were DOC-consuming events followed by low abundance of high-PCoA3 bacteria, which lasted until newly synthetized DOC joined the DOM pool. Increases in PCoA1 scores contributed to restore DOC levels, especially without shading (R^2=0.39 and p=0.001, Fig. S8). Moreover, PCoA3 was also associated with the availability of light for photosynthesis (K_{dPAR}), which has impacted PCoA1.

Taxonomic assignment

Figures 5 to 8 illustrate how the OTU richness of different bacterial groups changed in response to the main community drivers, as estimated by the first three PCoA axes. By evaluating the constraining effect of PCoA scores on taxa richness, we expected to obtain information on taxonomic adaptability in face of the observed changes in DOM pool. The dispersion of taxa richness over PCoA scores varied widely according to taxonomic level. As the PCoA scores varied widely over time (Fig. S9) and among treatments, the enrichment of taxa at specific ranges of PCoA scores indicated limited temporal and/or conditional occurrence (Figs. S10 to S13).

Overall, most phyla had OTU richness enlarged at low PCoA1 scores (Fig. 5). Within the four more abundant phyla, Actinobacteria and Verrucomicrobia were in line with this pattern, meanwhile among Proteobacteria and Bacteroidetes more OTUs with increased

PCoA1 were observed, suggesting enrichment at the final experimental days, especially in N^+ treatment (Fig. S10). At the class level, OTUs belonging to Alphaproteobacteria and Cytophagia achieved higher PCoA1 scores, whereas other classes like Spartobacteria, Acidimicrobiia and Clostridia were constrained to low scores (Fig. 6). Considering the observed association between PCoA1 and the proxies DOC and K_{dPAR}, taxa exhibiting high PCoA1 scores as Cytophagia are likely associated with active DOC production under increased availability of light at the PAR range. This distribution pattern was observed for OTUs associated with the family Rhodobacteraceae (Fig. 6) and the genus *Tabrizicola* (Fig. 8). Increases in DOC levels, water clarity (low K_{dPAR}) (Fig. 4), density of plastid-associated producers, and pH were all positively associated with PCoA1 (Fig. S14). As some of these associations were more predictable under full light (Figs. S8 and S15), an increase in CO_2 availability due to photo-oxidation might have contributed to the enhancement of productivity (as discussed by Tonetta et al., 2018), consequently favoring high-PCoA1 groups. Moreover, as the strongest declines in DOC levels occurred after rather than simultaneously to PCoA1 increases (Fig S16), the observed reduction in DOC levels was likely a consequence of DOM degradation by bacterial lineages exhibiting a pulse-like occurrence, like high-PCoA3 bacteria. Therefore, the associations between PCoA1 and the DOM pool resulted from the phytoplankton-associated production of autochthonous carbon rather than from a bacterioplankton-regulated process.

Axis 2 scores were low or intermediate for the dominant phyla. Actinobacteria (specially the Actinobacteria class) and Chloroflexi were remarkably enriched at low PCoA2 scores, suggesting that these phyla exhibited preferences for late non-supplemented conditions (Figs. 5 and 6). In contrast, Firmicutes (except for Bacilli class) was markedly enriched at high PCoA2 scores found at C^+ treatment on the initial stage of the experiment, thereby implying an association with allochthonous DOM input. Such OTU distribution

pattern was exhibited by the families Veillonellaceae, Ruminococcaceae and Clostridiaceae_1 (Firmicutes), likewise Sphingobacteriaceae (Bacteroidetes) (Fig. 7). Differently, three proteobacterial families (Oxalobacteraceae, Xanthomonadaceae and Pseudomonadaceae) distinctly presented reduction of OTUs as PCoA2 decreased. Regarding the PCoA2 association with qualitative CDOM proxies, these families were likely high molecular weight (HMW) carbon consumers supporting increases in $S_{275-295}$ and $S_{350-400}$. In contrast, most families presenting low PCoA2 as Sporichthyaceae, LD12, FukuN57 and Saprospiraceae likely showed preferences for low molecular weight (LMW) carbon and contributed to the reduction of the spectral slopes.

Like axis 1, most phyla exhibited low PCoA3 scores (Fig. 5). Notably, slightly increased scores were detected for Verrucomicrobia and Planctomycetes. Taxa showing increased PCoA3 scores as the Verrucomicrobial families Verrucomicrobiaceae and P. palm_C85 were likely involved in the PCoA3 peaks occurring on days 3 and 12 (Fig. 7). As assumed from the associations between PCoA3 and the DOM proxies, these taxa seem to play a role in CDOM consumption, reducing DOC levels and light attenuation in the PAR range. The regulation of DOC changes by bacteria linked with PCoA3 was stronger in nutrient supplemented treatments (Fig. S17). Verrucomicrobia *Prosthecobacter*, *Haloferula* and *Luteolibacter* were among genera that reached the highest PCoA3 values (Fig. 8), likely being typical representatives of this recycling lifestyle.

Discussion

Despite many previous studies have reported changes in BCS in response to DOM composition (Kritzberg et al., 2006; Judd et al., 2006; Gomez-Consarnau et al., 2012; Roiha et al., 2016; Smith et al., 2018), evidences for BCS influencing DOM characteristics are scarce (Guerrero-Feijóo et al., 2017; Goldberg et al., 2017; Wu et al., 2018). Our results

provide insights on links between observed changes in BCS and in the carbon pool, with community composition influencing and responding to specific DOM properties. Importantly, there was a strong influence of BCS on DOM processing and transformation, indicating that as some bacterial components use different substrates, they alter the DOM pool in specific ways. We also found that nutrients input was the main driver of bacterioplankton community and activity, either by enhancing microbial growth rates or through phytoplankton-DOM production, consistent with previous studies (Osterholz et al., 2016; Landa et al., 2016). Notably, our findings indicate that specific microbial members have potential impacts on changes in DOM pool molecular weight and suggest that a specific group, Verrucomicrobiaceae, plays a key role in CDOM turnover in these tropical waters.

Primary production as a driver of bacterial community changes

The most pronounced change in BCS (PCoA1) was caused by nutrient addition, which furthermore enhanced air-water fluxes of CO_2 and O_2 (Tonetta et al., 2018), pelagic metabolic rates (Brighenti et al., 2018) and autochthonous DOC levels (Brandão et al., 2018). Our results also showed that PCoA1 was a proxy of a nutrient-induced impoverishment of bacterial diversity (Figs. 5 to 8). During the experiment, the heterotrophic activity was likely constrained as soon as the initially available labile carbon was respired, which happened briefly under nutrient supplementation, as shown by the sudden decreases in pCO_2 after the second day (Tonetta et al., 2018). In turn, simultaneous increases in PCoA1 scores, DOC levels, frequencies of Cyanobacteria and chloroplasts, together with decreases in bacterioplankton frequency and evenness were observed after day three in N^+ treatments, indicating that a "heterotrophic collapse" had occurred. In this sense, most taxa exhibiting low PCoA1 scores (Figs. 5 to 8) were likely outcompeted by phytoplankton and phytoplankton-associated bacteria. In addition to the effects of DOM and nutrient additions on BCS, pelagic community metabolism, including background bacterial respiration, were

421 also greatly affected (Brighenti et al., 2018). This supports previous findings that the growth
422 rate of planktonic microorganisms is strongly depended on the availability of nutrients and
423 labile DOM, favoring fewer and faster growing bacterial species rather than more diverse
424 community under slower growth conditions (Sterner and Elser, 2002; Godwin and Cotner,
425 2014).

426 Our results indicate that the class-level OTU classification discriminates
427 phytoplankton-associated and/or fast-growing bacteria from groups with either limited
428 capacity to directly compete with phytoplankton, or incapable of thriving under high
429 productivity (Fig. 6). The latter represent the lake epilimnetic background community,
430 particularly enriched by Actinobacteria and Verrucomicrobia, which are abundant phyla in
431 Lake Carioca (Ávila et al., 2017). Moreover, a decrease in community evenness over time
432 was observed specially for N^+ treatments, indicating that a few lineages colonized during
433 periods of high primary production (*e.g.* classes Alphaproteobacteria and Cytophagia).
434 Members of Alphaproteobacteria, especially the Rhodobacteraceae family, and Cytophagia
435 have been consistently associated with phytoplankton-derived DOM (Eckert et al., 2012;
436 Sarmento et al., 2016; Bunse et al., 2016). Within these groups, genera associated with high-
437 PCoA1 scores, like *Tabrizicola*, have been found to be closely associated with phytoplankton
438 in a symbiotic lifestyle (Cui et al., 2017), supporting a tight relation between high-PCoA1
439 faster-growing lineages and primary producers. Lineages reaching high-PCoA1 scores were
440 likely supported by a carbon substrate that might not transform the DOM pool (Lucas et al.,
441 2016). Accordingly, bacteria associated with PCoA1 seems to involve fast-growing bacteria
442 capable of rapidly incorporating freshly produced phytoplankton exudates (Fouilland et al.,
443 2014). Indeed, preference for high concentrations of phytoplankton-derived DOM is
444 suggested by the positive link between PCoA1 and DOC levels (Fig. S8). Sarmento et al.
445 (2016) have shown that members of Bacteroidetes, which in our study exhibited high PCoA1

446 scores (classes Cytophagia and Flavobacteria), are more active with increasing
447 phytoplankton-DOM concentration.

448 **Changes in DOM quality and allochthonous DOM influence**

449 Shifts in BCS observed by the second principal component axis, PCoA2, were closely
450 related to indices of DOM quality. Such shifts were initially influenced by allochthonous
451 DOM addition, which induced notably high PCoA2 scores at day zero. However, nutrient
452 addition also imposed a late increase in PCoA2 scores, suggesting that the influence of BCS
453 on the qualitative DOM proxies $S_{350\text{-}400}$ and $S_{275\text{-}295}$ represent bacterial transformation of
454 phytoplankton-produced and terrigenous carbon. These proxies are useful for tracking
455 different pools of allochthonous and autochthonous DOM (Brandão et al., 2016). As $S_{350\text{-}400}$
456 and $S_{275\text{-}295}$ both record changes in carbon molecular size (Helms et al., 2008), the enrichment
457 of phyla exhibiting low PCoA2 scores, like Actinobacteria and Chloroflexi, likely contributed
458 to the augment of DOM molecular weight. In contrast, reduction of DOM molecular weight
459 resulted from the increased abundance of Saccharibacteria and Parcubacteria, which
460 presented high-PCoA2. Importantly, full light seems to have hindered the effect of these BCS
461 shifts on biodegradable DOM (Fig. S6), by blurring the association between changes in
462 PCoA2-associated bacteria (especially LMW carbon consumers, as Sporichthyaceae,
463 Saprospiraceae and FukuN57) and DOM quality. Oppositely, shading stimulated the bacterial
464 groups competing for substrate with the photo-transformation processes, thereby stabilizing
465 the influence of these taxa on DOM quality. Alternatively, an enhanced production of LMW
466 autochthonous DOM was likely favored by reduced photoinhibition of phytoplankton in
467 shaded treatments (Brighenti et al., 2018).

468 An alternative ecological interpretation of BCS shifts (here PCoA2), concerns the
469 early stage of the experiment, when communities in C^+ treatments showed remarkable
470 changes (Fig. S9). The inoculation of bacteria-containing allochthonous litter strongly

471 affected BCS in C^+ treatments until day three, when all treatments exhibited very similar
472 PCoA2 scores. Allochthonous bacteria were represented mainly by fermentative taxa
473 belonging to Firmicutes (*e.g.* Ruminoccocaceae and Veillonellaceae, Fig. 7) and other
474 lineages direct or indirectly associated with plant-polysaccharide degradation, as
475 Saccharibacteria and *Mucilaginibacter* (Figs. 5 and 8, respectively) (Pankratov et al., 2007;
476 Starr et al., 2018). Similarly to PCoA2 scores, OTU richness was immediately increased by
477 allochthonous DOM supplementation (Fig. 1) and then diminished, suggesting that PCoA2
478 also represented a strong selective pressure on allochthonous lineages in the lake. Therefore,
479 genera highly abundant on C^+ treatments on day zero, like *Sporomusa,* had OTUs condensed
480 at the higher limit of PCoA2 and were briefly cleared away, meanwhile *Burkholderia* has
481 thriven later, exhibiting lower values of PCoA2, suggesting a short but higher persistency
482 (Fig. 8). The rapid fading of inoculum-associated bacteria might have occurred due to high
483 oxygen levels, which has probably constrained the occurrence of obligate anaerobes and
484 microaerophiles within Clostridia and Negativicutes (Fig. 6) (Wiegel et al., 2006,
485 Marchandin et al., 2010). In contrast, lineages as *Burkholderia,* which were also initially
486 favoured by allochthonous DOM addition but resisted longer, were possibly benefited by its
487 ability to tolerate oxidative stress conditions and to thrive in association with photodegraded
488 organic matter (Paul et al., 2012). In comparison, the family level was more suitable than
489 genus for detecting gradual and homogeneous changes throughout PCoA2 scores, thus
490 allowing the recognition of taxa consistently contributing to the observed changes in DOM
491 quality. As an example, increased richness of Sporichthyaceae and FukuN57 occurred
492 downwards PCoA2 scores (Fig. 7). These taxa, together with the genera *Limnohabitans* and
493 Candidatus Aquirestis, which also exhibited low PCoA2 (Fig. 8), are considered consumers
494 of LMW carbon (Jones et al., 2009; Šimek et al., 2010; Eckert et al., 2012). In contrast,
495 usually assumed as copiotrophic microbes (Nelson and Carlson, 2012; Landa et al., 2013),

496 gammaproteobacteria (families Xanthomonadaceae and Pseudomonadaceae) and
497 Flavobacteriaceae presented enrichment at increasing PCoA2 scores, suggesting preference
498 for HMW DOM as also previously suggested by Amaral et al. (2016) and Orsi et al. (2016).
499 Importantly, Zhang et al. (2015) has shown that in oceanic waters, these groups are involved
500 in the degradation of HMW exopolysaccharides potentially resulting in production of humic-
501 like recalcitrant DOC, especially in replete N and P conditions. This could explain the
502 association between high PCoA2 scores and increases in SUVA observed under nutrient
503 supplementation (between days 0-3 and 9-12, Fig. 2), suggesting a participation of high-
504 PCoA2 lineages in DOM aromatization. Therefore, as shifts in BCS as described above
505 occur, they seem to affect and shape the DOM pool by depleting substrates of distinct
506 molecular weight, thus contributing to changes in spectral slopes and overall DOM quality.

507 **CDOM recycling**

508 The third principal component axis (PCoA3) was a component of the bacterioplankton
509 community highly committed to the observed changes in DOM pool (Fig. 4). Increases in
510 PCoA3 scores resulted in lower DOC levels, which were subsequently recovered after the
511 PCoA3 pulse (Table 4). The regulation of DOC changes by bacteria linked with PCoA3 were
512 more robust in nutrient supplemented treatments (Fig. S17), suggesting that either PCoA3-
513 associated bacteria recycle DOC under replete nutrient conditions, or present increased
514 specificity for substrates produced in N^+ treatments. Additionally, as larger changes in DOC
515 levels were more precisely predicted by PCoA3 under nutrient addition than in control,
516 bacteria associated with PCoA3 should incorporate or respire autochthonous DOC efficiently.
517 Also, as PCoA3 and 16S abundance simultaneously peaked on day 3, lineages exhibiting
518 high PCoA3 scores should achieve high cell counts, which might explain the efficiency in
519 regulating DOC levels and water transparency (Fig. 4). Our results also showed that
520 reduction of $S_{350\text{-}400}$ and increase of a_{350} induced high-PCoA3 bacteria under shading (Fig.

S7), suggesting that high-PCoA3 bacteria are active consumers of HMW, chromophoric DOC, which might be susceptible to photodegradation or have production hampered by photo-inhibition. Brandão et al. (2018) pointed out that during the experiment, autochthonous carbon production increased absorption at wavelengths above 350 nm, adding onto the contribution of freshly produced carbon on PCoA3. Intriguingly, our findings indicate that the Gammaproteobacteria-Flavobacteria (high-PCoA2) growth might have contributed to the PCoA3 pulses by producing HMW aromatic DOC, as high PCoA2 scores preceded pulses in PCoA3 (Fig. S9).

Our results showed that members of the Verrucomicrobiaceae family were enriched at high PCoA3 scores, notably OTUs associated with the genera *Prosthecobacter*, *Haloferula*, *Brevifollis* and *Luteolibacter* (Fig. 8). Although information concerning the roles of most verrucomicrobial groups in freshwater is still scarce, these genera have been found in different aquatic environments and their adaptive success rely on a broad repertoire of carbon-degrading enzymes (Martinez-Garcia et al., 2012; Zhang et al., 2014; Balmonte et al., 2016). Verrucomicrobiaceae have been previously associated with increases in phytoplankton-derived bioavailable DOM (Landa et al., 2013) and contribute to hydrolysis of complex HMW-polysaccharides (Cardman et al., 2014). Moreover, a metagenomic survey on freshwater Verrucomicrobia revealed an enrichment of Ton transporters genes (Cabello-Yeves et al., 2017), which code for proteins involved on complex HMW DOM cycling (McCarren et al., 2010). Therefore, our findings suggest that a few closely related lineages consume HMW DOM, most likely of autochthonous origin, indicating an ecologically coherent and exclusive role for Verrucomicrobiaceae in our experiment. This finding contributes to the current knowledge of bacterial taxa involved in the degradation of complex microbial-produced DOM, as data on microbial populations responsible for cycling recalcitrant DOM are still scarce (Zhang et al., 2018).

The DOM aspects linked to high-PCoA3 values concerned not only carbon quality (a_{350} and $S_{350-400}$), but also decreased levels of DOC and PAR attenuation. This suggests that high-PCoA3 bacteria likely impacted water transparency, increasing light availability at wavelengths >400 nm, resulting in a subsequent increased primary productivity and abundance of phototrophs. Likewise, high-PCoA3 bacteria seem to reduce the aromaticity of the DOM pool (SUVA decrease). Thus, high PCoA3-groups like Verrucomicrobiaceae, *Chthonomonas* (Armatimonadetes), *Parafilimonas* (Chitinophagaceae), *Oceanicoccus* (Gammaproteobacteria) and *Aquabacterium* (Betaproteobacteria) seem to be highly active in recycling DOM. Our results indicate that these bacteria are capable of sensing DOM changes (Fig. S7) and as response, controlling the CDOM fate (quantitatively and qualitatively) by efficiently consuming the accumulated aromatic HMW fraction of the DOM pool, impacting light availability and other community members, specially DOC producers.

Conclusions

Our results revealed consistent associations between distinct microbial groups and specific changes in the DOM pool over time, suggesting resource partitioning among bacterial groups, as previously reported for the microbial organic matter turnover in the sea (McCarren et al., 2010). We observed a dynamic control of community members on DOM fate, with specialized groups affecting distinct properties of DOM, likely contributing altogether to DOM recycling. The activity of each specialized group was time-dependent: as productivity increased and carbon molecular weight decreased, active consumers of HMW carbon and/or fast-growing strains were gradually replaced by other bacterial groups with affinity for LMW compounds. This exchange occurred concomitantly with a pulse of DOC-consuming, notably Verrucomicrobiaceae, showing preference for chromophoric carbon of autochthonous origin. Some lineages, as Flavobacteriaceae and Gammaproteobacteria might

have contributed to the production of such complex chromophoric DOM pool. Although the succession pattern described above also occurred in the control (Fig. S9), increasing DOM and nutrient resources enhanced the magnitude of the microbial shifts, likely due to an augmented availability of substrate leading to a higher abundance of the favored groups. Lineages tightly linked to autochthonous carbon production (PCoA1) reflected this trend quantitatively, changing proportionally to the density of primary producers, which imposed a high restrain on background communities. Moreover, the switch between Flavobacteria-Gammaproteobacteria and Sporichthyaceae-LD12 groups seems to regulate DOM quality, and distinguished bacterial groups based on molecular weight affinity.

Therefore, our findings claim attention for a verrucomicrobial family (Verrucomicrobiaceae) and other taxa as *Chthonomonas* and *Aquabacterium* as short-lived but yet important recyclers of DOM affecting water clarity and re-fueling primary production. These findings expand the basis for future investigations aiming to deep the comprehension of DOM cycling in tropical lakes, which might validate the efficiency of these microbial players as major lineages responsible for CDOM remineralization. Finally, our study confirms that different sources of DOM impact specific bacterial groups differently. More importantly, our findings suggest that taxonomically defined assemblages play definite roles when influencing DOM fate, either by changing specific fractions of the DOM pool or by regulating DOC levels.

Acknowledgements

This work was supported by the Fundação de Amparo à Pesquisa do Estado de Minas Gerais (FAPEMIG); Conselho Nacional de Desenvolvimento Científico e Tecnológico (CNPq); and Coordenação de Aperfeiçoamento de Pessoal de Nível Superior (CAPES) through the project Carbon Cycling in Lakes (COCLAKE – CAPES Proc. no 88881.030499/2013-01). We would

like to thank Gustavo Turci, Patrícia Ferreira and Ralph Thomé for field support. We also thank Diego Pujoni for his valuable suggestions and Anderson Carmo for the support during DNA sequencing at LBMM-ICB-UFMG.

Figure legends

Figure 1: Temporal variation of alpha diversity (OTU richness and evenness – Simpson 1/D), 16S copy number, and percentages of bacterioplankton, cyanobacteria and chloroplast-associated reads. Values represent means ± SE. Red and black colours depict treatments with and without allochthonous DOM addition, respectively. Triangle and circle symbols correspond to treatments with and without nutrient addition, respectively. Solid lines represent shaded treatments and dashed lines indicate full light.

Figure 2: Temporal variation of a_{350}, $S_{275-295}$, $S_{350-400}$, dissolved organic carbon (DOC), SUVA and K_{dPAR}. Values represent means ± SE. Red and black colours depict treatments with and without allochthonous DOM addition, respectively. Triangle and circle symbols correspond to treatments with and without nutrient addition, respectively. Solid lines represent shaded treatments and dashed lines indicate full light.

Figure 3: Temporal variation of PCoA1, 2 and 3. Values represent means ± SE. Red and black colours depict treatments with and without allochthonous DOM addition, respectively. Triangle and circle symbols correspond to treatments with and without nutrient addition, respectively. Solid lines represent shaded treatments and dashed lines indicate full light.

Figure 4: Diagram illustrating the synchronism between shifts in bacterioplankton community structure and DOM proxies. Detailed statistics are shown on Tables 4 and 5.

621 Quantitative, quantitative/qualitative and qualitative proxies are represented by ellipses,
622 triangles and rectangles, respectively. Red and green lines represent negative and positive
623 associations, respectively. Solid and dashed lines represent significant linearity between a
624 three-day shift ($\Delta PCoA^{0-3}$ and ΔDOM^{0-3}) and the associated explanatory variable
625 immediately before ($PCoA^{0}$ and DOM^{0}), or after ($PCoA^{3}$ and DOM^{3}) the shift, respectively.
626 Black and yellow stars represent increased fitness of the association under shading and full-
627 light, respectively.
628
629 **Figure 5:** Ternary plot showing all OTUs of 12 different phyla chosen to represent distinct
630 patterns of occurrence in relation to the three main PCoA axis. Each circle represents one
631 OTU positioned according to the normalized contribution of the indicated PCoA axis (species
632 score): PCoA1 + PCoA2 + PCoA3 = 1 (100%). Colored areas depict the density (Gaussian
633 kernel estimator) of the OTUs distribution. The number between parenthesis indicates the
634 total richness of OTUs for each phylum.
635
636 **Figure 6:** Ternary plot showing all OTUs of 12 different classes chosen to represent distinct
637 patterns of occurrence in relation to the three main PCoA axis. Each circle represents one
638 OTU positioned according to the normalized contribution of the indicated PCoA axis (species
639 score): PCoA1 + PCoA2 + PCoA3 = 1 (100%). Colored areas depict the density (Gaussian
640 kernel estimator) of the OTUs distribution. The number between parenthesis indicates the
641 total richness of OTUs for each class.
642
643 **Figure 7:** Ternary plot showing all OTUs of 16 different families chosen to represent distinct
644 patterns of occurrence in relation to the three main PCoA axis. Each circle represents one
645 OTU positioned according to the normalized contribution of the indicated PCoA axis (species

score): PCoA1 + PCoA2 + PCoA3 = 1 (100%). Colored areas depict the density (Gaussian kernel estimator) of the OTUs distribution. The number between parenthesis indicates the total richness of OTUs for each family.

Figure 8: Ternary plot showing all OTUs of 16 different genera chosen to represent distinct patterns of occurrence in relation to the three main PCoA axis. Each circle represents one OTU positioned according to the normalized contribution of the indicated PCoA axis (species score): PCoA1 + PCoA2 + PCoA3 = 1 (100%). Colored areas depict the density (Gaussian kernel estimator) of the OTUs distribution. The number between parenthesis indicates the total richness of OTUs for each genus.

References

Amaral, V., Graeber, D., Calliari, D., Alonso, C., 2016. Strong linkages between DOM optical properties and main clades of aquatic bacteria. Limnol. Oceanogr. 61: 906–918.

Amon, R.M.W., Benner, R., 1994. Rapid cycling of high-molecular-weight dissolved organic matter in the ocean. Nature. 369: 549–552.

Asmala, E., Haraguchi, L., Carstensen, J., Jakobsen, H., Massicotte, P., 2018. Nutrient availability as major driver of phytoplankton- derived dissolved organic matter transformation in coastal environment. Biogeochemistry. 137: 93–104.

Ávila, M.P., Staehr, P.A., Barbosa, F.A.R., Chartone-Souza, E., Nascimento, A.M.A., 2017. Seasonality of freshwater bacterioplankton diversity in two tropical shallow lakes from the Brazilian Atlantic Forest. FEMS Microbiol. Ecol. 93: 10.1093/femsec/fiw218

667 Barbosa, L.G, Barbosa, F.A.R., Bicudo, C.E.M., 2012. Inter-annual chemical stratification in
668 Brazilian natural lakes: meromixis and hypolimnetic memory. Acta Limnologica Brasiliensia.
669 24: 127–139.

670 Balmonte, J.P., Arnosti, C., Underwood, S., Mckee, B.A., 2016. Riverine bacterial
671 communities reveal environmental disturbance signatures within the Betaproteobacteria and
672 Verrucomicrobia. Front. Microbiol. 7: 1441.

673 Benner, R. 2002. Chemical composition and reactivity. 59–90. Biogeochemistry of marine
674 dissolved organic matter, Elsevier Science.

675 Benner, R., Amon, R.M.W., 2015. The size-reactivity continuum of major bioelements in the
676 ocean. Annu. Rev. Mar. Sci. 7: 185–205.

677 Berggren, M., Laudon, H., Jansson, M., 2009. Aging of allochthonous organic carbon
678 regulates bacterial production in unproductive boreal lakes, Limnol. Oceanogr. 54: 1333–
679 1342.

680 Berglund, J., Müren, U., Båmstedt, U., Andersson, A., 2007. Efficiency of a phytoplankton-
681 based and a bacteria-based food web in a pelagic marine system. Limnol. Oceanogr. 52: 121
682 – 131.

683 Bezerra-Neto, J.F., Brighenti, L.S., Pinto-Coelho, R.M., 2010. A new morphometric study of
684 Carioca Lake, Parque Estadual do Rio Doce (PERD), Minas Gerais State, Brazil. Acta Sci
685 Biol Sci. 32: 49–54.

686 Bocaniov, S.A., Barton, D.R., Schiff, S.L., Smith, R.E.H., 2013. Impact of tributary DOM
687 and nutrient inputs on the nearshore ecology of a large, oligotrophic lake (Georgian Bay,
688 Lake Huron, Canada). Aquat. Sci. 75: 321–332.

689 Brandão, L.P.M., Staehr, P.A., Bezerra-Neto, J.F., 2016. Seasonal changes in optical
690 properties of two contrasting tropical freshwater systems. J. Limnol. 75: 18.

691 Brandão, L.P.M., Brighenti, L.S., Staehr, P.A., Asmala, E., Massicotte, P., Tonetta, D.,
692 Barbosa, F.A.R., Pujoni, D., et al., 2018. Distinctive effects of allochthonous and
693 autochthonous organic matter on CDOM spectra in a tropical lake. Biogeosciences. 15:
694 2931–2943.

695 Brighenti, L.S., Staehr, P.A., Gagliardi, L.M., Brandão, L.P.M., Elias, E.C., de Mello,
696 N.A.S.T., Barbosa, F.A.R., Bezerra-Neto, J.F., 2015. Seasonal changes in metabolic rates of
697 two tropical lakes in the Atlantic Forest of Brazil. Ecosystems. 18: 589–604.

698 Brighenti, L.S., Staehr, P.A., Brandão, L.P.M., Barbosa, F.A.R., Bezerra-Neto, J.F., 2018.
699 Importance of nutrients, organic matter and light availability on epilimnetic metabolic rates in
700 a mesotrophic tropical lake. Freshwater Biol. 63: 1143–1160.

701 Bunse, C., Bertos-Fortis, M., Sassenhagen, I., Sildever, S., Sjöqvist, C., Godhe, A., Gross, S.,
702 Kremp, A., et al., 2016. Spatio-temporal interdependence of bacteria and phytoplankton
703 during a baltic sea spring bloom. Front. Microbiol. 7: 517. doi: 10.3389/fmicb.2016.00517

704 Cabello-Yeves, P.J., Ghai, R., Mehrshad, M., Picazo, A., Camacho, A., Rodriguez-Valera, F.,
705 2017. Reconstruction of diverse verrucomicrobial genomes from metagenome datasets of
706 freshwater reservoirs. Front. Microbiol. 8: 2131. doi: 10.3389/fmicb.2017.02131

707 Cardman, Z., Arnosti, C., Durbin, A., Ziervogel, K., Cox, C., Steen, A.D., Teske, A., 2014.
708 Verrucomicrobia are candidates for polysaccharide-degrading bacterioplankton in an Arctic
709 fjord of Svalbard. Appl. Environ. Microbiol. 80: 3749–3756.

710 Carpenter, S.R., Stanley, E.H., Zanden, M.J.V., 2011. State of the world's freshwater
711 ecosystems: physical, chemical, and biological changes. Annu. Rev. Environ. Resour. 36: 75–
712 99.

713 Cory, R.M., Kling, G.W., 2018. Interactions between sunlight and microorganisms influence
714 dissolved organic matter degradation along the aquatic continuum. Limnol. Oceanogr.
715 Letters. 3: 102–116.

716 Cotner, J.B., Biddanda, B.A., 2002. Small players, large role: microbial influence on
717 biogeochemical processes in pelagic aquatic ecosystems. Ecosystems. 5: 105–121.

718 Cui, Y., Jin, L., Ko, S.R., Chun, S.J., Oh, H.S., Lee, C.S., Srivastava, A., Oh, H.M., et al.,
719 2017. Periphyton effects on bacterial assemblages and harmful cyanobacterial blooms in a
720 eutrophic freshwater lake: a mesocosm study. Sci. Rep. 7: 7827.

721 De Haan, H., De Boer, T., 1987. Applicability of light absorbance and fluorescence as
722 measures of concentration and molecular size of dissolved organic carbon in humic Laken
723 Tjeukemeer. Water Res. 21: 731–734.

724 Eckert, E.M., Salcher, M.M., Posch, T., Eugster, B., Pernthaler, J., 2012. Rapid successions
725 affect microbial N-acetyl-glucosamine uptake patterns during a lacustrine spring
726 phytoplankton bloom. Environ. Microbiol. 14: 794–806.

727 Edgar, R.C., Haas, B.J., Clemente, J.C., Quince, C., Knight, R., 2011. UCHIME improves
728 sensitivity and speed of chimera detection. Bioinformatics 27: 2194–2200.

729 Evans, J., Sheneman, L., Foster J.A., 2006. Relaxed Neighbor-Joining: A Fast Distance-
730 Based Phylogenetic Tree Construction Method. J. Mol. Evol. 62: 785-792.

731 Farjalla, V.F., Marinho, C.C., Faria, B.M., Amado, A.M., Esteves, F.D.A., Bozelli, R.L.,
732 Giroldo, D., 2009. Synergy of fresh and accumulated organic matter to bacterial growth.
733 Microb. Ecol. 57: 657–666.

734 Fonte, E.S., Amado, A.M., Meirelles-Pereira, F., Esteves, F.A., Rosado, A.S., Farjalla, V.F.,
735 2013. The combination of different carbon sources enhances bacterial growth efficiency in
736 aquatic ecosystems. Microb. Ecol. 6: 871–878.

737 Fouilland, E., Tolosa, I., Bonnet, D., Bouvier, C., Bouvier, T., Bouvy, M., Got, P., Le Floc'h,
738 E., et al., 2014. Bacterial carbon dependence on freshly produced phytoplankton exudates
739 under different nutrient availability and grazing pressure conditions in coastal marine waters.
740 FEMS Microbiol. Ecol. 87: 757–769.

741 Godwin, C.M., Cotner, J.B., 2014. Carbon:phosphorus homeostasis of aquatic bacterial
742 assemblages is mediated by shifts in assemblage composition. Aquat. Microb. Ecol. 73: 245–
743 258.

744 Goldberg, S.J., Nelson, C.E., Viviani, D.A., Shulse, C.N., Church, M.J., 2017. Cascading
745 influence of inorganic nitrogen sources on DOM production, composition, lability and
746 microbial community structure in the open ocean. Environ. Microbiol. 19: 3450–3464.

747 Gomez-Consarnau, L., Lindh, M.V., Gasol, J.M., Pinhassi, J., 2012. Structuring of
748 bacterioplankton communities by specific dissolved organic carbon compounds. Environ.
749 Microbiol. 14: 2361–2378.

750 Guerrero-Feijóo, E., Nieto-Cid, M., Sintes, E., Dobal-Amador, V., Hernando-Morales, V.,
751 Álvarez, M., Balagué, V., Varela, M.M., 2017. Optical properties of dissolved organic matter

752 relate to different depth-specific patterns of archaeal and bacterial community structure in the
753 North Atlantic Ocean. FEMS Microbiol. Ecol. 93: 1–14.

754 Hamilton, N.E., Ferry, M., 2018. "ggtern: Ternary Diagrams Using ggplot2." Journal of
755 Statistical Software, Code Snippets, 87: 1–17.

756 Hansen, A.M., Kraus, T.E.C., Pellerin, B.A., Fleck, J.A., Downing, B.D., Bergamaschi, B.A.,
757 2016. Optical properties of dissolved organic matter (DOM): Effects of biological and
758 photolytic degradation. Limnol. Oceanogr. 61: 1015–1032.

759 Helms, J.R., Stubbins, A., Ritchie, J.D., Minor, E.C., Kieber, D.J., Mopper, K., 2008.
760 Absorption spectral slopes and slope ratios as indicators of molecular weight, source, and
761 photobleaching of chromophoric dissolved organic matter. Limnol. Oceanogr. 53: 955–969.

762 Jansson, M., Persson, L., De Roos, A.M., Jones, R.I., Tranvik, L.J., 2007. Terrestrial carbon
763 and intraspecific size-variation shape lake ecosystems. Trends in Ecology & Evolution. 22:
764 316–22.

765 Jones, S.E., Newton, R.J., McMahon, K.D., 2009. Evidence for structuring of bacterial
766 community composition by organic carbon source in temperate lakes. Environ. Microbiol. 11:
767 2463–72.

768 Judd, K.E., Crump, B.C., Kling, G.W., 2006. Variation in dissolved organic matter controls
769 bacterial production and community composition. Ecology. 87: 2068–2079.

770 Kirk, J.T.O., 1994. Light and photosynthesis in aquatic ecosystems. Cambridge University
771 Press.

772 Klindworth, A., Pruesse, E., Schweer, T., Peplies, J., Quast, C., Horn, M., Glöckner, F.O.,
773 2013. Evaluation of general 16S ribosomal RNA gene PCR primers for classical and next-
774 generation sequencing-based diversity studies. Nucleic Acids Research. 41(1): e1. doi:
775 10.1093/nar/gks808

776 Kritzberg, E.S., Langenheder, S., Lindström, E.S., 2006. Influence of dissolved organic
777 matter source on lake bacterioplankton structure and function - Implications for seasonal
778 dynamics of community composition. FEMS Microbiol. Ecol. 56: 406–417.

779 Landa, M., Cottrell, M.T., Kirchman, D.L., Blain, S., Obernosterer, I., 2013. Changes in
780 bacterial diversity in response to dissolved organic matter supply in a continuous culture
781 experiment. Aquat. Microb. Ecol. 69: 157–168.

782 Landa, M., Blain, S., Christaki, U., Monchy, S., Obernosterer, I., 2016. Shifts in bacterial
783 community composition associated with increased carbon cycling in a mosaic of
784 phytoplankton blooms. ISME J. 10: 39–50.

785 Lane, D.J., 1991. 16S/23S rRNA sequencing (pp. 115–175). In E. Stackebrandt, & M.
786 Goodfellow (Eds.), Nucleic acid techniques in bacterial systematics, New York, USA: John
787 Wiley and Sons.

788 Lindeman, R.L., 1942. The trophic-dynamic aspect of ecology. Ecology. 23: 399–418.

789 Lozupone, C., Knight, R., 2005. UniFrac: a new phylogenetic method for comparing
790 microbial communities. App. Environ. Microbiol. 71: 8228–8235.

791 Lucas, J., Koester, I., Wichels, A., Niggemann, J., Dittmar, T., Callies, U., Wiltshire, K.H.,
792 Gerdts, G., 2016. Short-term dynamics of North Sea bacterioplankton-dissolved organic
793 matter coherence on molecular level. Front. Microbiol. 7: 1–14.

794 Marchandin, H., Teyssier, C., Campos, J., Jean-Pierre, H., Roger, F., Gay, B., Carlier, J.P.,
795 Jumas-Bilak, E., 2010. *Negativicoccus succinicivorans* gen. nov., sp. nov., isolated from
796 human clinical samples, emended description of the family Veillonellaceae and description of
797 Negativicutes classis nov., Selenomonadales ord. nov. and Acidaminococcaceae fam. nov. in
798 the bacterial phylum Firmicutes. Int. J Syst. Evol. Microbiol. 60: 1271–1279.

799 Martinez-Garcia, M., Brazel, D.M., Swan, B.K., Arnosti, C., Chain, P.S., Reitenga, K.G.,
800 Xie, G., Poulton, N.J., et al., 2012. Capturing single cell genomes of active polysaccharide
801 degraders: an unexpected contribution of Verrucomicrobia. PLoS One. 7: e35314.

802 Massicotte, P., Asmala, E., Stedmon, C., Markager, S., 2017. Global distribution of dissolved
803 organic matter along the aquatic continuum: Across rivers, lakes and oceans. Sci. Tot.
804 Environ. 609: 180–191.

805 McCarren, J., Becker, J.W., Repeta, D.J., Shi, Y., Young, C.R., Malmstrom, R.R., Chisholm,
806 S.W., DeLong, E.F., 2010. Microbial community transcriptomes reveal microbes and
807 metabolic pathways associated with dissolved organic matter turnover in the sea. Proc. Natl.
808 Acad. Sci. 107: 16420–16427.

809 McKnight, D.M., Andrews, E.D., Spaulding, S.A., Aiken, G.R., 1994. Aquatic fulvic acids in
810 algal-rich antarctic ponds. Limnol. Oceanogr. 39: 1972–1979.

811 McMurdie, P.J., Holmes, S., 2013. phyloseq: an R package for reproducible interactive
812 analysis and graphics of microbiome census data. PLoS ONE. 8(4): e61217.

813 Muyzer, G., de Waal, E.C., Uitterlinden, G., 1993. Profiling of complex microbial
814 populations by denaturing gradient gel electrophoresis analysis of polymerase chain reaction-
815 amplified genes coding for 16S rRNA. Appl. Environ. Microbiol. 59: 695–700.

816 Nelson, C.E., Carlson, C.A., 2012. Tracking differential incorporation of dissolved organic
817 carbon types among diverse lineages of Sargasso Sea bacterioplankton. Environ. Microbiol.
818 14: 1500–1516.

819 Nelson, N.B., Carlson, C.A., Steinberg, D.K., 2004. Production of chromophoric dissolved
820 organic matter by Sargasso Sea microbes. Mar. Chem. 89: 273–287.

821 Orsi, W.D., Smith, J.M., Liu, S., Liu, Z., Sakamoto, C.M., Wilken, S., Poirier, C., Richards,
822 T.A., 2016. Diverse, uncultivated bacteria and archaea underlying the cycling of dissolved
823 protein in the ocean. ISME J. 10: 2158–2173.

824 Osterholz, H., Singer, G., Wemheuer, B., Daniel, R., Simon, M., Niggemann, J., Dittmar, T.,
825 2016. Deciphering associations between dissolved organic molecules and bacterial
826 communities in a pelagic marine system. ISME J. 10: 1717–1730.

827 Pankratov, T.A., Tindall, B.J., Liesack, W., Dedysh, S.N., 2007. *Mucilaginibacter paludis*
828 gen. nov., sp. nov. and *Mucilaginibacter gracilis* sp. nov., pectin-, xylan and laminarin-
829 degrading members of the family Sphingobacteriaceae from acidic Sphagnum peat bog. Int.
830 J. Syst. Evol. Microbiol. 57: 2349–2354.

831 Paul, A., Dziallas, C., Zwirnmann, E., Gjessing, E.T., Grossart, H.P., 2012. UV irradiation of
832 natural organic matter (NOM): Impact on organic carbon and bacteria. Aquat. Sci. 74: 443–
833 454.

834 Paulson, J.N., Stine, O.C., Bravo, H.C., Pop, M., 2013. Differential abundance analysis for
835 microbial marker-gene surveys. Nature Methods. 10: 1200–1202.

836 Pernthaler, J., 2005. Predation on prokaryotes in the water column and its ecological
837 implications. Nat. Rev. Microbiol. 3: 537–547.

838 Quast, C., Pruesse, E., Yilmaz, P., Gerken, J., Schweer, T., Yarza, P., Peplies, J., Glöckner,
839 F.O., 2013. The SILVA ribosomal RNA Gene Database Project: improved data processing
840 and web-based tools. Nucleic Acids Research. 41(Database issue): D590–D596. https:
841 //doi.org/10.1093/nar/gks1219

842 Reis, M.P., Barbosa, F.A.R., Chartone-Souza, E., Nascimento, A.M.A., 2013. The
843 prokaryotic community of a historically mining-impacted tropical stream sediment is as
844 diverse as that from a pristine stream sediment. Extremophiles. 17: 301–309.

845 Reis, P.C.J., Martinelli, L.A., Barbosa, F.A.R., 2016. Basal carbon sources and planktonic
846 food web in a tropical lake: an isotopic approach. Mar. Freshwater Res. 68: 429-441.

847 Rochelle-Newall, E., Delille, B., Frankignoulle, M., Gattuso, J.P., Jacquet, S., Riebesell, U.,
848 Terbruggen, A., Zondervan, I., et al., 2004. Chromophoric dissolved organic matter in
849 experimental mesocosms maintained under different pCO2 levels. Mar. Ecol. Prog. Ser. 272:
850 25–31.

851 Roiha, T., Peura, S., Cusson, M., Rautio, M., 2016. Allochthonous carbon is a major
852 regulator to bacterial growth and community composition in subarctic freshwaters. Sci. Rep.
853 6: 1–12.

854 Sanders, R.W., Cooke, S.L., Fischer, J.M., Fey, S.B., Heinze, A.W., Jeffrey, W.H., A.L.,
855 Macaluso, Moellert, R.E., et al., 2015. Shifts in microbial food web structure and productivity
856 after additions of naturally occurring dissolved organic matter: Results from large-scale
857 lacustrine mesocosms. Limnol. Oceanogr. 60: 2130–2144.

Sarmento, H., Morana, C., Gasol, J.M., 2016. Bacterioplankton niche partitioning in the use of phytoplankton-derived dissolved organic carbon: quantity is more important than quality. ISME J. 10: 2582-2592.

Schloss, P.D., Westcott, S.L., Ryabin, T., Hall, J.R., Hartmann, M., Hollister, E.B., Lesniewski, R.A., Oakley, B.B., et al., 2009. Introducing mothur: Open-source, platform-independent, community-supported software for describing and comparing microbial communities. Appl. Environ. Microbiol. 75: 7537–7541.

Šimek, K., Kasalický, V., Jezbera, J., Jezberová, J., Hejzlar, J., Hahn, M.W., 2010. Broad habitat range of the phylogenetically narrow R-BT065 cluster, representing a core group of the betaproteobacterial genus limnohabitans. Appl. Environ. Microbiol. 76: 631–639.

Smith, H.J., Dieser, M., McKnight, D.M., SanClements, M.D., Foreman, C.M., 2018. Relationship between dissolved organic matter quality and microbial community composition across polar glacial environments. FEMS Microbiol. Ecol. 94: 1–10.

Starr, E.P., Shi, S., Blazewicz, S.J., Probst, A.J., Herman, D.J., Firestone, M.K., Banfield, J.F., 2018. Stable isotope informed genome-resolved metagenomics reveals that Saccharibacteria utilize microbially-processed plant-derived carbon. Microbiome 6: 1–12.

Sterner, R.W., Elser, J.J., 2002. Ecological Stoichiometry: The biology of elements from molecules to the Biosphere. Princeton University Press, Princeton.

Tonetta, D., Staehr, P.A., Obrador, B., Brandão, L.P.M., Brighenti, L.S., Petrucio, M.M., Barbosa, F.A.R., Bezerra-Neto, J.F., 2018. Effects of nutrients and organic matter inputs in the gases CO_2 and O_2: A mesocosm study in a tropical lake. Limnologica. 69: 1–9.

879 Weishaar, J.L., Aiken, G.R., Bergamaschi, B.A., Fram, M.S., Fujii, R., Mopper, K., 2003.
880 Evaluation of specific ultraviolet absorbance as an indicator of the chemical composition and
881 reactivity of dissolved organic carbon. Environ. Sci. Technol. 37: 4702–4708.

882 Wickham, H., 2016. ggplot2: elegant graphics for data analysis. Springer New York.

883 Wiegel, J., Tanner, R., Rainey, F.A., 2006. An introduction to the family Clostridiaceae. In
884 The Prokaryotes: a handbook on the biology of bacteria, 3rd edn, vol. 4, pp. 654–678. Edited
885 by M. Dworkin, S. Falkow, E. Rosenberg, K. H. Schleifer & E. Stackebrandt. Springer: New
886 York.

887 Wu, X., Wu, L., Liu, Y., Zhang, P., Li, Q., Zhou, J., Hess, N.J., Hazen, T.C., et al., 2018.
888 Microbial interactions with dissolved organic matter drive carbon dynamics and community
889 succession. Front. Microbiol. 9: 1–12.

890 Zhang, C., Dang, H., Azam, F., Benner, R., Legendre, L., Passow, U., Polimene, L.,
891 Robinson, C., et al., 2018. Evolving paradigms in biological carbon cycling in the ocean.
892 National Science Review. 5: 481–499.

893 Zhang, J., Zhang, X., Liu, Y., Xie, S., Liu, Y., 2014. Bacterioplankton communities in a high-
894 altitude freshwater wetland. Ann. Microbiol. 64: 1405–1411.

895 Zhang, Z., Chen, Y., Wang, R., Cai, R., Fu, Y., Jiao, N., 2015. The fate of marine bacterial
896 exopolysaccharide in natural marine microbial communities. PLoS One. 10: 1–16.

897

898 **Figures**

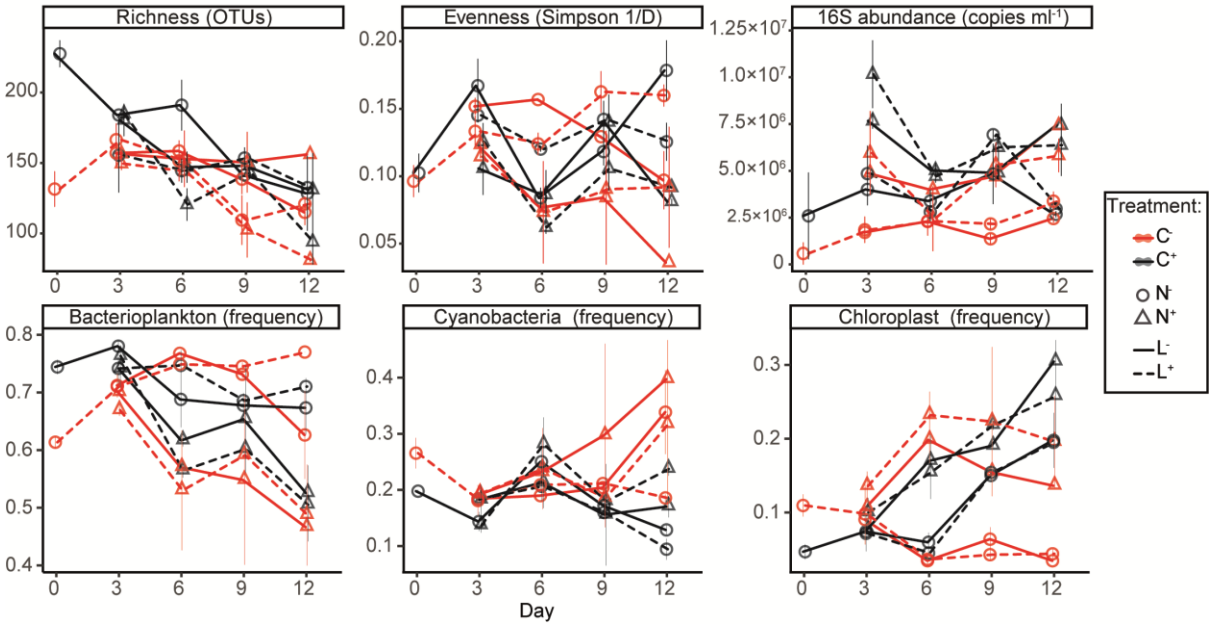

899

900 Figure 1.

901

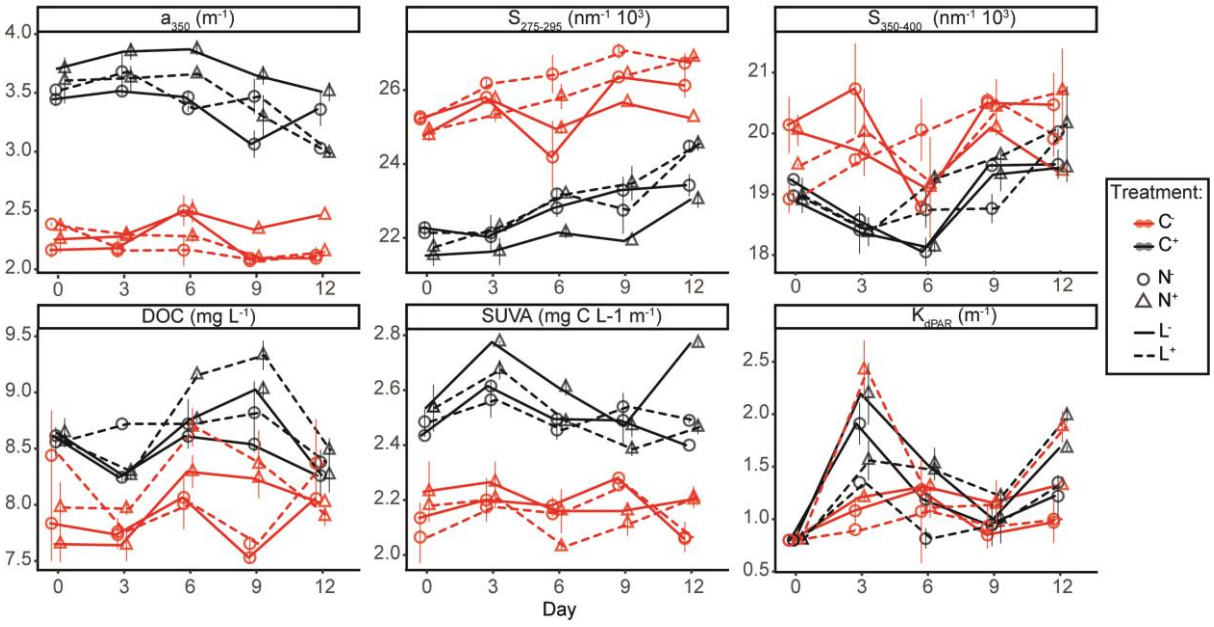

902

903 Figure 2.

904

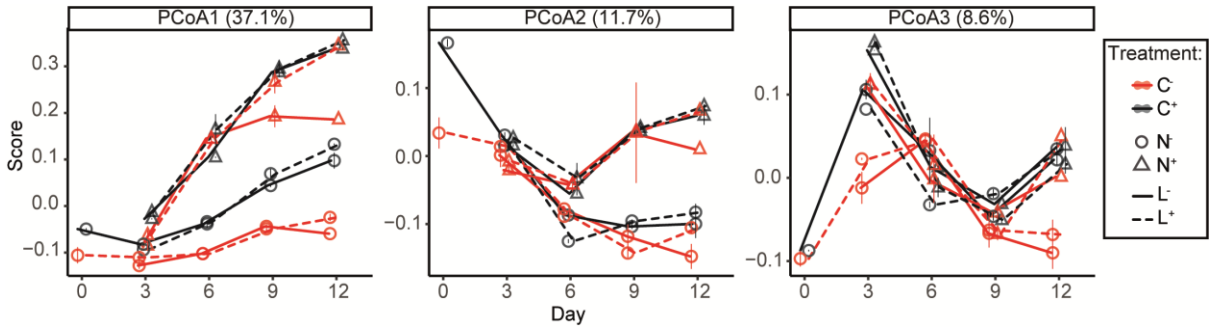

905

906 Figure 3.

907

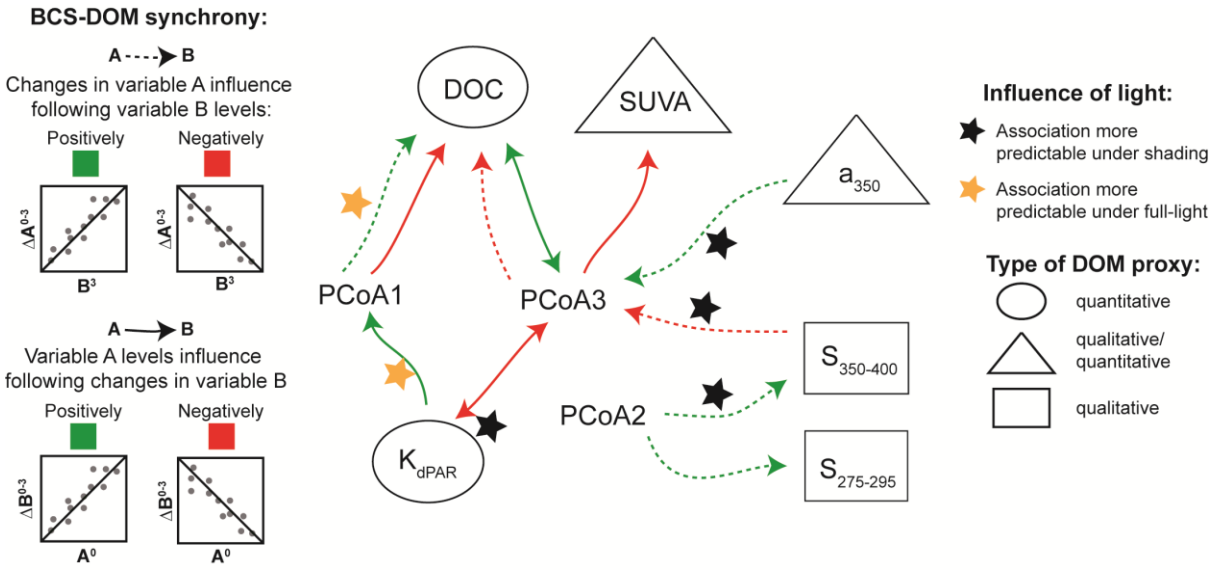

908

909 Figure 4.

910

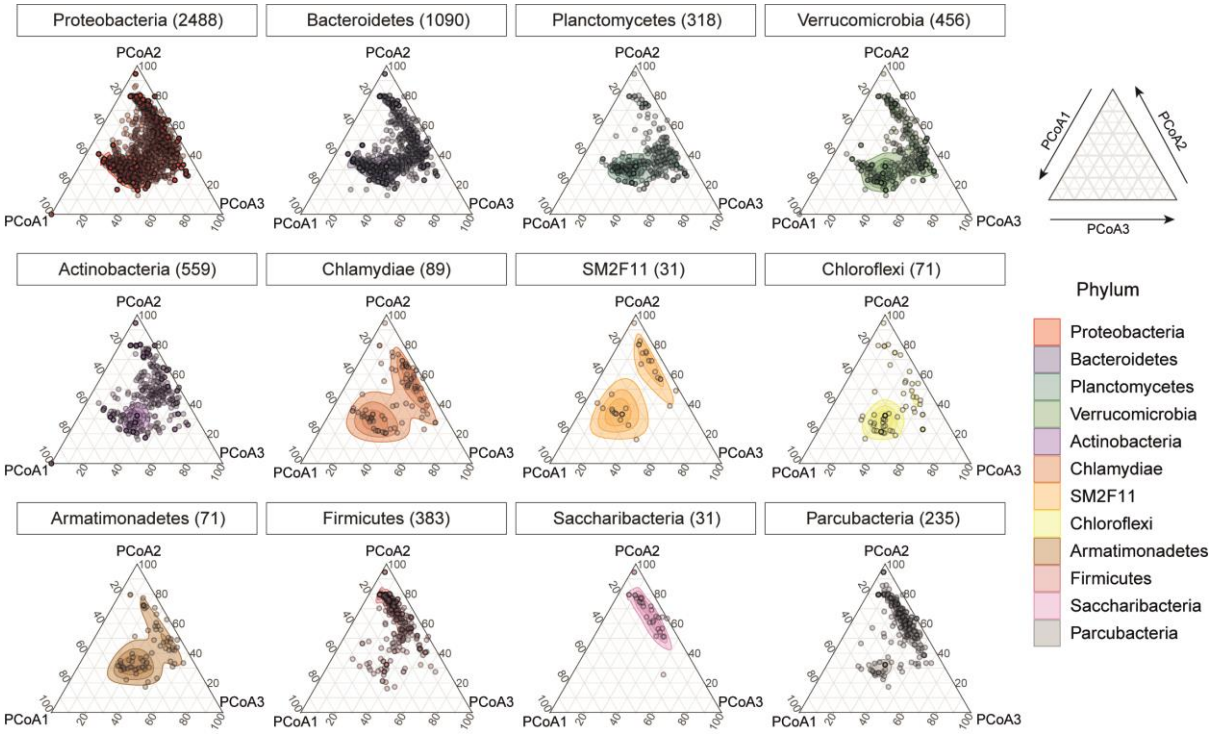

911

912 Figure 5.

913

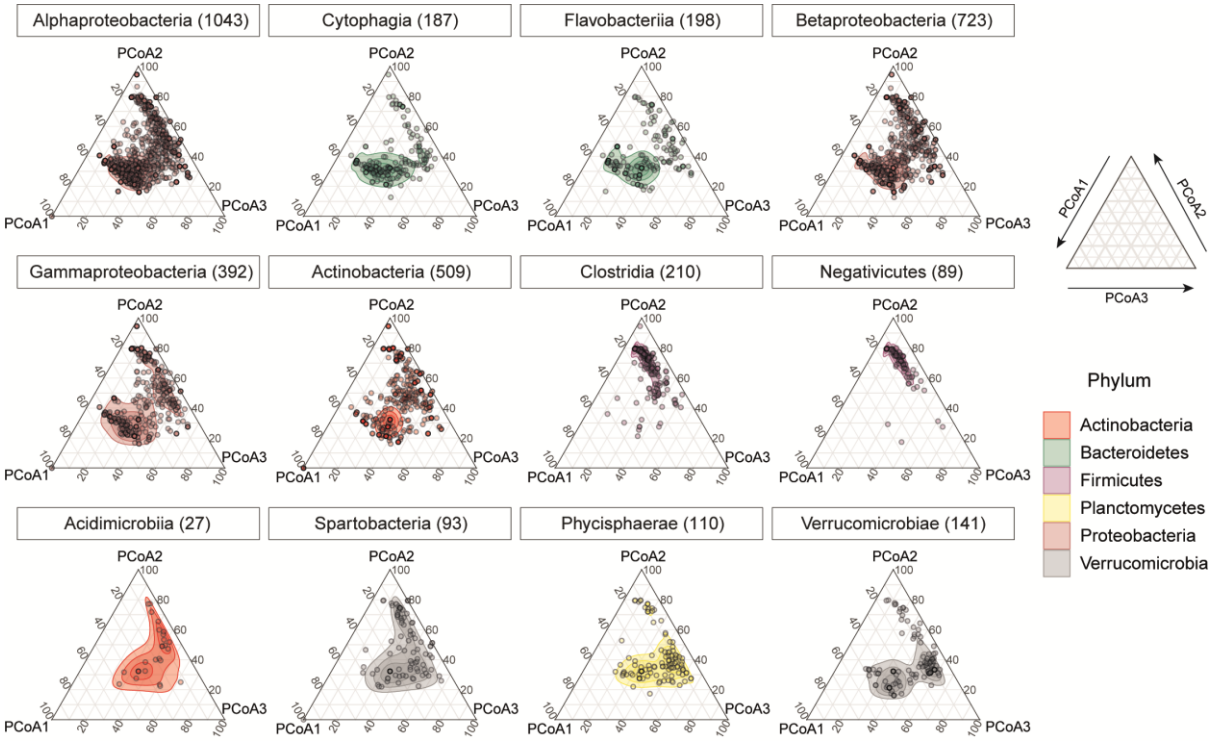

914

915 Figure 6.

916

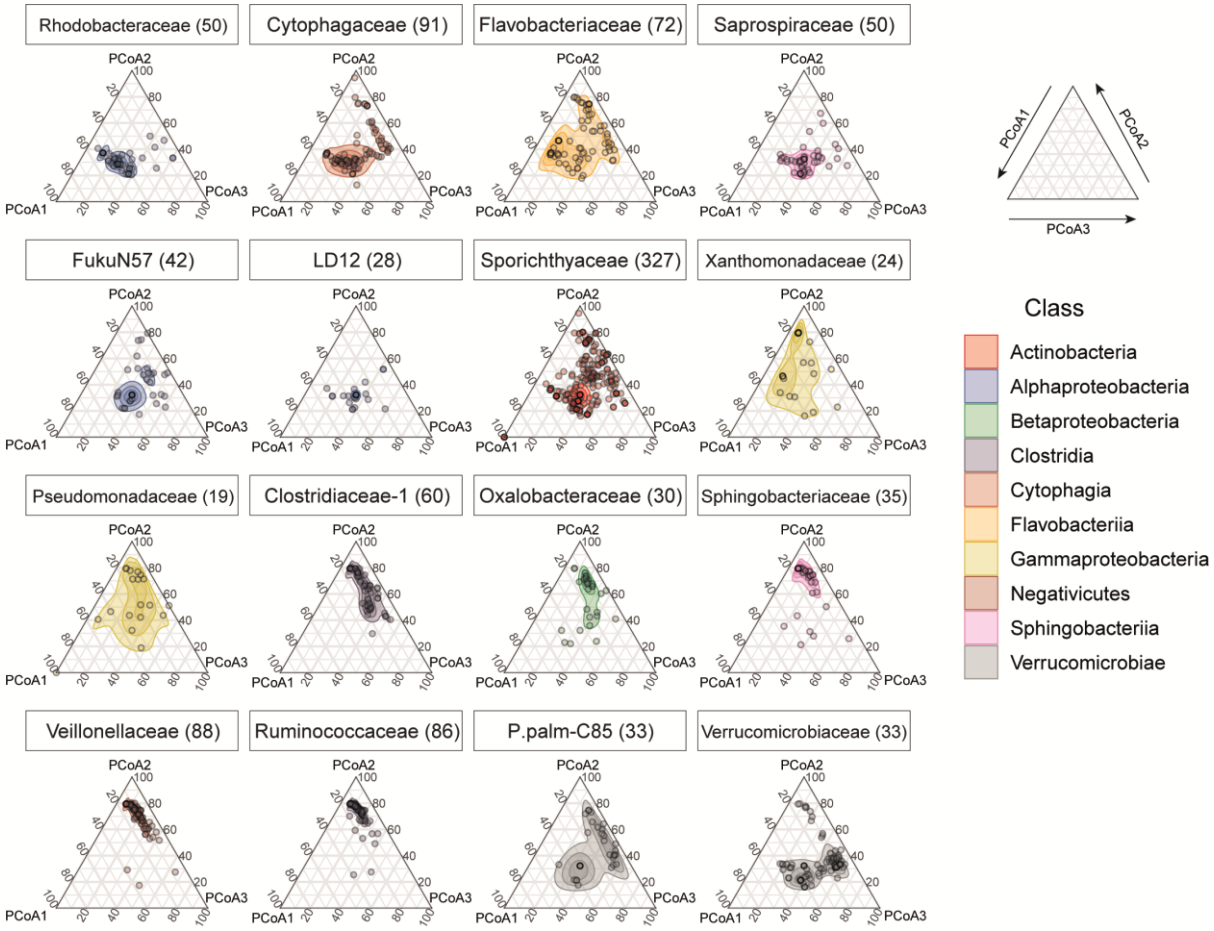
Rhodobacteraceae (50)
Cytophagaceae (91)
Flavobacteriaceae (72)
Saprospiraceae (50)
FukuN57 (42)
LD12 (28)
Sporichthyaceae (327)
Xanthomonadaceae (24)
Pseudomonadaceae (19)
Clostridiaceae-1 (60)
Oxalobacteraceae (30)
Sphingobacteriaceae (35)
Veillonellaceae (88)
Ruminococcaceae (86)
P.palm-C85 (33)
Verrucomicrobiaceae (33)
PCoA1
PCoA2
PCoA3
Class
Actinobacteria
Alphaproteobacteria
Betaproteobacteria
Clostridia
Cytophagia
Flavobacteriia
Gammaproteobacteria
Negativicutes
Sphingobacteriia
Verrucomicrobiae

Figure 7.

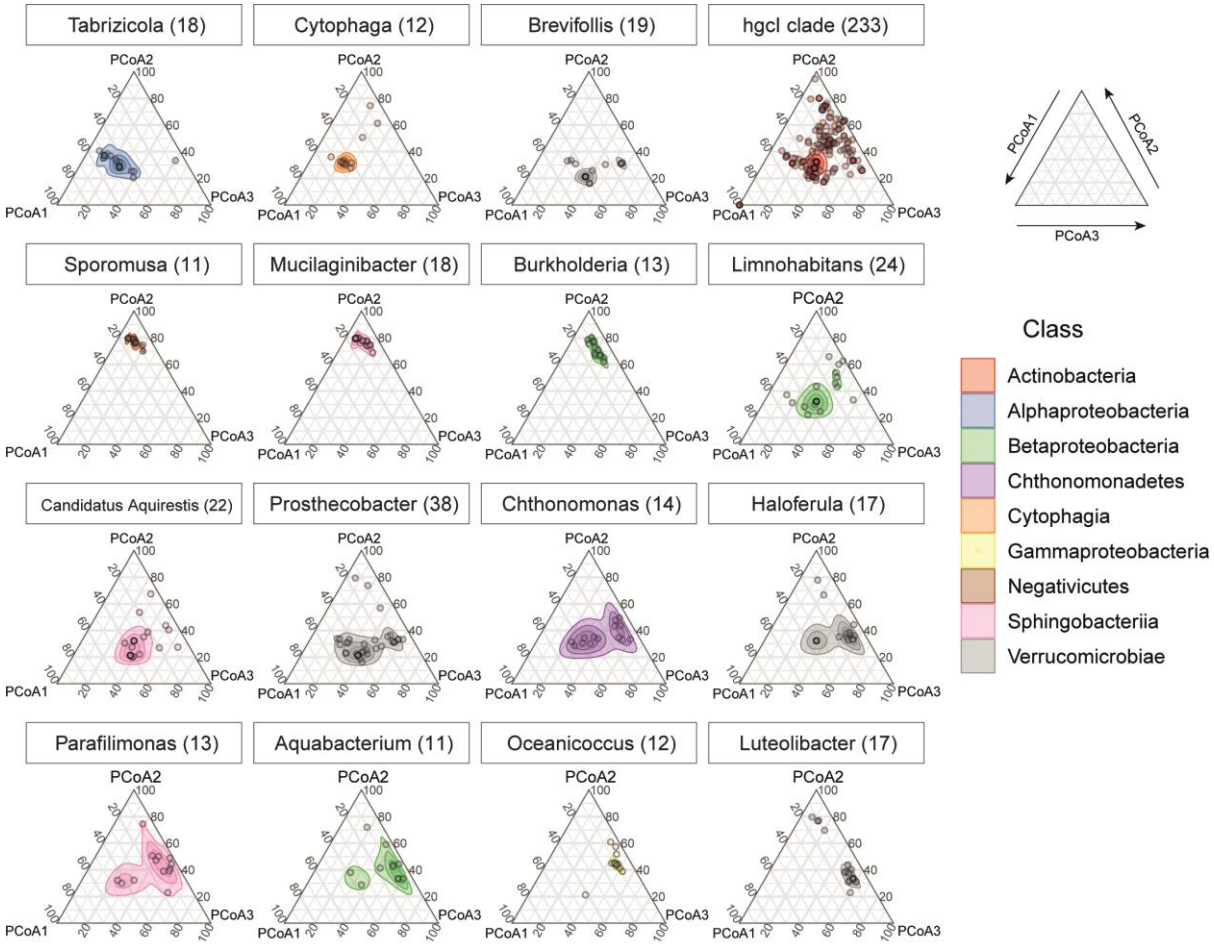
Tabrizicola (18)
Cytophaga (12)
Brevifollis (19)
hgcl clade (233)
Sporomusa (11)
Mucilaginibacter (18)
Burkholderia (13)
Limnohabitans (24)
Candidatus Aquirestis (22)
Prosthecobacter (38)
Chthonomonas (14)
Haloferula (17)
Parafilimonas (13)
Aquabacterium (11)
Oceanicoccus (12)
Luteolibacter (17)
PCoA1
PCoA2
PCoA3
Class
Actinobacteria
Alphaproteobacteria
Betaproteobacteria
Chthonomonadetes
Cytophagia
Gammaproteobacteria
Negativicutes
Sphingobacteriia
Verrucomicrobiae

Figure 8.

Tables

Table 1: Multiple linear regressions results, displaying the effect of the manipulations as mean overall changes and changes per day (indicated by the interaction of the manipulation with time) on 16S abundance, bacterioplankton richness and evenness and the relative frequency of bacterioplankton, cyanobacteria and chloroplasts.

			Allochthonous DOM addition	Nutrient addition	Shading	Combined addition
	adj R^2	change per day (control)	overall change/ daily change	overall change/ daily change	overall change	overall change
16S abundance	0.48	-	+331.0% [***]/ -19.3% [.]	+291.1% [**]/ -	-	-
Richness	0.55	-1.9% [*]	+25.5% [**]/ -	-	+15.1% [.]	-
Evenness	0.22	-	-	-/ -3.1% [.]	-	-
Bacterioplankton	0.56	-	-	-/ -2.9% [***]	-	-
Cyanobacteria	0.19	-	-/ -5.8% [*]	-/ +5.3% [*]	-	-
Chloroplasts	0.72	-5.0% [.]	-86.0% [**]/ +18.0% [****]	+65.3% [*]/ +8.4% [**]	-	-53.4% [*]

Non-significant effects are indicated by a dash symbol "-". 16S abundance accounted for bacterioplankton, cyanobacteria and chloroplasts together. The symbols [.], [*], [**], [***], [****] indicates the p-value of each regression as marginally significant (0.1-0.05), 0.05-0.01, 0.01-$10E^{-3}$, $10E^{-3}$-$10E^{-5}$, $<10E^{-5}$, respectively.

Table 2: Multiple linear regressions results, displaying the effect of the manipulations as mean overall changes and changes per day (indicated by the interaction of the manipulation with time) on dissolved organic carbon (DOC), aromaticity (SUVA), absorbance at 350 nm (a_{350}) and the spectral slopes between 275-295nm ($S_{275-295}$) and 350-400nm ($S_{350-400}$).

			Allochthonous DOM addition	Nutrient addition	Shading	Nutrient addition shaded
	adj R^2	change per day (control)	overall change/ daily change	overall change/ daily change	overall change/ daily change	overall change
DOC	0.45	-	+8.7% [***]/ -	-	-	-
SUVA	0.79	-	+17.2% [****]/ -	+3.9% [.]/ -	-	-
a_{350}	0.94	-0.96% [**]	+56.5% [****]/ -1.1% [**]	+9.1% [*]/ -	-7.7% [*]/ -	+9.1% [**]
$S_{275-295}$	0.91	+0.2% [.]	-13.3% [****]/ +0.2% [.]	-2.2% [*]/ -	-/ -0.3% [**]	-
$S_{350-400}$	0.42	-	-6.5% [**]/ -	-	+3.7% [*]/ -0.4% [*]	-2.6% [.]

Non-significant effects are indicated by a dash symbol "-". The symbols [.], [*], [**], [***], [****] indicates the p-value of each regression as marginally significant (0.1-0.05), 0.05-0.01, 0.01-$10E^{-3}$, $10E^{-3}$-$10E^{-5}$, <$10E^{-5}$, respectively.

Table 3: Multiple linear regressions results, displaying the effect of the manipulations as mean overall changes and changes per day (indicated by the interaction of the manipulation with time) on the main principal coordinates PCoA1, PCoA2 and PCoA3.

				Allochthonous DOM addition	Nutrient addition	Shading	Combined addition
	% of community variance	adj R^2	change per day (control)	overall change/ daily change	overall change/ daily change	daily change	overall change
PCoA1	37.1%	0.93	+10.5% [*]	+67.4% [.]/+11.7% [**]	-/ +42.4% [****]	-	-83.9% [**]
PCoA2	11.7%	0.68	-7.3% [****]	-	-41.0% [***]/ +9.2% [****]	-2.5% [.]	-
PCoA3	8.6%	0.25	-	-	+75.3% [***]/ -6.8% [**]	-	-

The percentage of variance explained by each axis is also displayed. Non-significant effects are indicated by a dash symbol "-". The symbols [.], [*], [**], [***], [****] indicates the p-value of each regression as marginally significant (0.1-0.05), 0.05-0.01, 0.01-$10E^{-3}$, $10E^{-3}$-$10E^{-5}$, <$10E^{-5}$, respectively.

Table 4: Effect of BCS on DOM. Results of the of linear regressions tested between DOM proxies and BCS, which was evaluated as changes in scores of the three main PCoA's axes within three-day intervals. The results show significant associations (p-value < 0.05, R^2 > 0.2) about changes in BCS that determine DOM fate ($\Delta PCoA^{0\text{-}3} \sim DOM^3$) and changes in DOM pool that are determined by a previous community ($\Delta DOM^{0\text{-}3} \sim PCoA^0$).

Changes in BCS determine DOM						**BCS determines changes in DOM**					
All treatments + control											
$\Delta PCoA^{0\text{-}3}$ (y)	**DOM^3 (x)**	***intercept***	***coef.***	***R^2***	***p-value***	**$\Delta DOM^{0\text{-}3}$ (y)**	**$PCoA^0$ (x)**	***intercept***	***coef.***	***R^2***	***p-value***
PCoA1	**DOC**	-0.570	0.077	0.273	1.65E-04	**DOC**	**PCoA3**	-0.022	3.783	0.288	1.02E-04
						SUVA	**PCoA3**	-0.003	-0.845	0.217	0.001
Only treatments											
$\Delta PCoA^{0\text{-}3}$ (y)	**DOM^3 (x)**	***intercept***	***coef.***	***R^2***	***p-value***	**$\Delta DOM^{0\text{-}3}$ (y)**	**$PCoA^0$ (x)**	***intercept***	***coef.***	***R^2***	***p-value***
PCoA2	**$S_{275\text{-}295}$**	-0.546	0.022	0.213	0.007	**DOC**	**PCoA1**	0.164	-2.757	0.442	2.47E-05
PCoA2	**$S_{350\text{-}400}$**	-1.152	0.059	0.385	1.17E-04	**DOC**	**PCoA3**	-0.114	5.290	0.657	1.07E-08
PCoA3	**DOC**	1.073	-0.128	0.244	0.003	**SUVA**	**PCoA3**	0.026	-1.345	0.589	3.02E-07
PCoA3	**K_{dPAR}**	-0.208	0.139	0.219	0.006						

Table 5: Effect of DOM on BCS. Results of the of linear regressions tested between DOM proxies and BCS, which was evaluated as changes in scores of the three main PCoA's axes within three-day intervals. The results show significant associations (p-value < 0.05, R^2 > 0.2) about changes in DOM that determine BCS fate ($\Delta DOM^{0\text{-}3}$ ~ $PCoA^3$) and changes in BCS that are determined by a previous DOM pool ($\Delta PCoA^{0\text{-}3}$ ~ DOM^0).

Changes in DOM determine BCS						**DOM determines changes in BCS**					
All treatments + control											
						$\Delta PCoA^{0\text{-}3}$ (y)	**DOM^0 (x)**	***intercept***	***coef.***	***R^2***	***p-value***
						PCoA1	**K_{dPAR}**	-0.035	0.089	0.344	1.82E-05
						PCoA3	**K_{dPAR}**	0.120	-0.111	0.299	8.45E-05
Only treatments											
$\Delta DOM^{0\text{-}3}$ (y)	**$PCoA^3$ (x)**	***intercept***	***coef.***	***R^2***	***p-value***	**$\Delta PCoA^{0\text{-}3}$ (y)**	**DOM^0 (x)**	***intercept***	***coef.***	***R^2***	***p-value***
$S_{350\text{-}400}$	**PCoA3**	0.276	-10.168	0.286	0.001	**PCoA1**	**K_{dPAR}**	0.002	0.071	0.251	0.003
						PCoA3	**DOC**	-0.932	0.106	0.207	0.008
						PCoA3	**K_{dPAR}**	0.146	-0.125	0.372	2.08E-04